


Article

Comparative Study of Pd–Ni Bimetallic Catalysts Supported on UiO-66 and UiO-66-NH₂ in Selective 1,3-Butadiene Hydrogenation

Lili Liu ¹, Lei Yu ¹, Xiaojing Zhou ¹, Chunling Xin ¹, Songyuan Sun ¹, Zhidong Liu ¹, Jinyu Zhang ², Ying Liu ^{1,*} and Xishi Tai ^{1,*}

¹ School of Chemistry & Chemical Engineering and Environmental Engineering, Weifang University, Weifang 261061, China; liulili122@wfu.edu.cn (L.L.); jimoyulei@163.com (L.Y.); zhouxiaojing105@wfu.edu.cn (X.Z.); 20150015@wfu.edu.cn (C.X.); ssy1210661650@foxmail.com (S.S.); liuzhidong0518@foxmail.com (Z.L.)

² Shandong Huazhiyuan Testing Co., Ltd., Weifang 261061, China; ziyjinyu@163.com

* Correspondence: liuying@wfu.edu.cn (Y.L.); taixs@wfu.edu.cn (X.T.)

Abstract: Selective hydrogenation of 1,3-butadiene (BD) is regarded as the most promising route for removing BD from butene streams. Bimetallic Pd–Ni catalysts with changed Pd/Ni molar ratios and monometallic Pd catalysts were synthesized using two differently structured metal-organic framework supports: UiO-66 and UiO-66-NH₂. The effects of the structure of support and the molar ratio of Pd/Ni on the catalytic property of selective BD hydrogenation were studied. The Pd–Ni bimetallic supported catalysts, PdNi/UiO-66 (1:1) and PdNi/UiO-66-NH₂ (1:1), exhibited fine catalytic property at low temperature. Compared with UiO-66, UiO-66-NH₂ with a certain number of alkaline sites could reduce the catalytic activity for the BD hydrogenation reaction. However, the alkaline environment of UiO-66-NH₂ is helpful to improve the butene selectivity. PdNi/UiO-66-NH₂ (1:1) catalyst presented better stability than PdNi/UiO-66 (1:1) under the reaction conditions, caused by the strong interaction between the –NH₂ groups of UiO-66-NH₂ and PdNi NPs. Moreover, the PdNi/UiO-66-NH₂ (1:1) catalyst presented good reproducibility in the hydrogenation of BD. These findings afford a beneficial guidance for the design and preparation of efficient catalysts for selective BD hydrogenation.

Keywords: Pd–Ni bimetallic catalysts; UiO-66; UiO-66-NH₂; 1,3-butadiene hydrogenation



Citation: Liu, L.; Yu, L.; Zhou, X.; Xin, C.; Sun, S.; Liu, Z.; Zhang, J.; Liu, Y.; Tai, X. Comparative Study of Pd–Ni Bimetallic Catalysts Supported on UiO-66 and UiO-66-NH₂ in Selective 1,3-Butadiene Hydrogenation. *Nanomaterials* **2022**, *12*, 1484. <https://doi.org/10.3390/nano12091484>

Academic Editors: Vincenzo Vaiano and Olga Sacco

Received: 8 April 2022

Accepted: 23 April 2022

Published: 27 April 2022

Publisher's Note: MDPI stays neutral with regard to jurisdictional claims in published maps and institutional affiliations.



Copyright: © 2022 by the authors. Licensee MDPI, Basel, Switzerland. This article is an open access article distributed under the terms and conditions of the Creative Commons Attribution (CC BY) license (<https://creativecommons.org/licenses/by/4.0/>).

1. Introduction

Butenes are key raw materials for polymer synthesis [1–3]. However, the butene streams produced from petroleum cracking contains small amounts of 1,3-butadiene (BD), which must be removed in the subsequent polymerization processing because it could cause catalyst poisoning and product quality degradation in downstream processes [4,5]. Selective BD hydrogenation is regarded as the most promising route for removing BD from butene streams [6,7]. In the past few decades, various catalysts, such as Au [8], Pt [9], Cu [10], Co [11], Pd [12], Pd–Au [13,14], Pd–Cu [1], Pd–Ag [15,16], Pd–Ni [17], Au–Ni [18], and Pt–Cu [19], have been developed and used in BD hydrogenation. Among them, bimetallic supported catalysts displayed excellent catalytic property for BD hydrogenation due to the synergistic effect between metals [17,18]. Lucci et al. [19] found that bimetallic PtCu/Al₂O₃ catalyst displayed 99% butene selectivity at 100% BD conversion. Lu et al. [15] showed that AgPd/g-Al₂O₃ catalysts displayed excellent BD conversion (98.2%) and butene selectivity (88.1%) in BD hydrogenation. Pattamakomsan et al. [6] reported that PdSn/Al₂O₃ catalysts not only have high 1-butene selectivity, but could also avoid deep hydrogenation and isomerization.

The support has a considerable effect on the catalytic performance for the selective BD hydrogenation reaction [20–25]. The interactions among metal NPs and supports, charging transfers, and support acidity play important roles in the catalytic activity and

product selectivity in BD hydrogenation [20,21]. Huang et al. [20] found that Pd1/graphene displayed higher activity than Pd1/C₃N₄ in the hydrogenation of BD. Hou et al. [21] investigated the impact of oxide supports on the BD hydrogenation over Pd–Ni bimetallic catalysts. They found that the chemical property of oxide support had no effect on activity of the catalyst, but it did have a significant effect on 1-butene selectivity because of the tough metal–support interaction and oxygen defects [21]. Decarolis et al. [22] also reported that the support type had a great influence on the catalytic property in BD selective hydrogenation.

Recently, the metal atomic ratio of bimetallic catalysts has been observed to affect the catalytic performance [7,26–30]. Méndez et al. [29] found that adding Ni to the Pd based catalysts decreased the hydrogenation activity (BD conversion) and improved the selectivity of the total butene at moderate BD conversions. The 1NiPd/Al₂O₃ catalyst (Pd = 0.5 wt%, Ni/Pd molar ratio of 1) exhibited improved catalytic performance for the BD selective hydrogenation [29]. Lonergan et al. [26] studied the effects of Pt:Ni atomic ratio of PtNi/γ-Al₂O₃ on the hydrogenation of BD. They observed that the catalysts having a lower Pt:Ni atomic ratio presented elevated catalytic activity [31]. Odoom-Wubah et al. [7] reported that Pd–Cu_{0.06}/Mn₂O₃-SI (SI = sol-immobilization) showed an effective balance between BD conversion and butene selectivity at room temperature. The catalyst Au(2)Pd(1)/MIL-101(Cr) displayed the best hydrogenation performance in the selective BD hydrogenation [31].

Metal–organic frameworks (MOFs) are greatly regular porous coordination polymers that have been widely used as a support in heterogeneous catalysts due to their large pore volumes and uniform cavities [32–34]. Bimetallic nanoparticle (NP) catalysts supported on MOF have been recently reported [35–38]. For instance, a ZIF-8 supported core-shell Ag@Au bimetallic catalyst (Ag@Au/ZIF-8) exhibited high conversion and selectivity of benzaldehyde in benzyl alcohol oxidation [38]. Au-Pd/MIL-101(Cr) NP catalysts displayed improved catalytic activity for BD hydrogenation [31]. Ni–Pt NPs supported on MIL-101-NH₂ displayed a good activity with a 137 h^{−1} turnover frequency (TOF) when hydrazine hydrate completely converted into hydrogen at 25 °C [36]. Ten et al. [39] also found that AgPd/UiO-66 catalysts showed good catalytic activity in propylene glycol oxidation due to the synergistic interaction between the components in Ag–Pd alloyed NPs. They also found that the catalytic activity was largely dependent on the preparation process and the properties of the metal precursors [39]. The AgPd/UiO-66 catalyst prepared by the double solvent method with aqueous nitrate salts as precursors and N₂H₄ reduction displayed the highest propylene glycol conversion [39].

Among the various reported MOFs, the UiO-66 series is an outstanding one for its high surface area, as well as its good chemical resistance to organic solvents and water and high thermal stability (>500 °C) [40,41]. In addition, the UiO-66 derivatives series, i.e., UiO-66-OH, UiO-66-COOH, UiO-66-NH₂, and UiO-66-NO₂, can be obtained through ligand functionalization [42,43]. Among them, UiO-66 and UiO-66-NH₂ have recently attracted great interest and have been widely used in adsorption and separation [44,45], luminescent sensing [46], antibacterial and antiviral [47], and catalytic reactions [48]. Especially, UiO-66 and UiO-66-NH₂ have been used as a support for metal NPs in catalyzing cinnamaldehyde hydrogenation [48], acetic acid hydrogenation [49], phenol hydrogenation [40], and CO₂ hydrogenation [50]. However, there are few studies about the effect of UiO-66 and UiO-66-NH₂ on the catalytic properties in BD hydrogenation. It has been reported that the basic and acidic nature of the support could markedly affect the general butene distribution and selectivity of 1-butene [5,51]. Acidic supports were less selective to the total butenes and inhibited the 1-butene selectivity [5,51]. In the present work, the catalytic property of UiO-66 and UiO-66-NH₂-supported Pd–Ni bimetallic NPs or Pd NPs in the selective BD hydrogenation reaction was compared and investigated. The effect of support structures and the Pd/Ni molar ratio of the catalysts PdNi/UiO-66 and PdNi/UiO-66-NH₂ on the catalytic activity and selectivity were studied. PdNi/UiO-66 displayed higher activity than PdNi/UiO-66-NH₂ in BD hydrogenation. However, PdNi/UiO-66-NH₂ displayed improved selectivity to total butenes and stability due to the interaction among PdNi NPs

and support. Furthermore, the Pd/Ni molar ratio of bimetallic Pd–Ni catalysts had a significant effect on the activity and product selectivity.

2. Experimental Section

2.1. Synthesis of UiO-66-NH₂ and UiO-66

The UiO-66-NH₂ crystal was prepared via the solvothermal method [52]. ZrCl₄ (2.40 mmol, 0.56 g) was melted into N,N'-dimethylformamide (DMF, 9 mL) under intense stirring. The 2-aminoterephthalic acid (NH₂-BDC, 5.10 mmol, 0.92 g) and benzoic acid (72.06 mmol, 8.80 g) were melted into 20 mL DMF. Afterwards, the DMF solution of ZrCl₄ was added into the solution of NH₂-BDC and benzoic acid. After stirring for 1 h, the homogenized solution was heated at 180 °C in a 100 mL Teflon autoclave for 24 h in a drying oven. The light-yellow powder was collected by centrifugation at 3800 rpm for 20 min. The powder was washed four times with DMF and methanol, respectively. Finally, it was dried for 24 h in a vacuum oven at 60 °C. UiO-66 was also prepared via the solvothermal method by using the same procedure, except using terephthalic acid (BDC) instead of NH₂-BDC.

2.2. Synthesis of Pd–Ni Bimetallic Catalysts

Pd–Ni bimetallic catalysts were synthesized via the impregnation method using Ni(NO₃)₂·6H₂O and Pd(CH₃COO)₂ as precursors [31]. First, Ni(NO₃)₂·6H₂O (0.086 mmol, 25.0 mg) and Pd(CH₃COO)₂ (0.086 mmol, 19.2 mg) were dissolved into 1 mL absolute ethanol. Second, the mixture of Ni(NO₃)₂·6H₂O and Pd(CH₃COO)₂ was added to UiO-66-NH₂ (0.3 g) drop by drop. The samples were ultrasonically treated at 20 °C for 1 h and then aged in the refrigerator at 4 °C for 24 h, followed by drying in a vacuum oven at 50 °C for 2 h. Finally, they were reduced in the H₂ stream (12.0 mL/min) at 50 °C for 2 h and labeled as PdNi/UiO-66-NH₂ (1:1). PdNi/UiO-66-NH₂ catalysts with Pd:Ni molar ratios of 1:3, 1:2, 1:1, 2:1, and 3:1 were synthesized for investigating the effects of Pd:Ni molar ratio on the activity and selectivity of BD hydrogenation, with a total metal (Pd and Ni) content of ca. 4.0 wt.% (Table S1). A series of PdNi/UiO-66 catalysts with Pd:Ni molar ratios of 1:3, 1:2, 1:1, 2:1, and 3:1 was also prepared via the impregnation method (Table S1). The Pd/UiO-66 and Pd/UiO-66-NH₂ catalysts were also synthesized via the impregnation method using Pd(CH₃COO)₂ as precursor (Table S1).

2.3. Catalytic Activity Measurement

The catalytic property of Pd–Ni NP and Pd NP supported catalysts was assessed using a continuous flowing system with a 6 mm inner diameter of quartz fixed-bed reactor under atmospheric pressure. Initially, 5 mg of fine powder catalyst was diluted with 0.5 g quartz sand (25–40 mesh), then placed at the center of the quartz reactor. The reactants, H₂ (6.5 mL/min) and BD/N₂ (1.0 vol.%, 20 mL/min), passed through the fixed catalyst bed with a space velocity of 318,000 mL/(h·g_{cat}) at 40–110 °C. The high space velocity can eliminate significant mass-transfer limitation during the hydrogenation of BD. The reactor effluent was measured online using the Al₂O₃ capillary column.

3. Results and Discussion

3.1. Characterization of Catalysts

The MOF supports and Pd–Ni bimetallic catalysts were investigated in detail by CO₂-TPD, PXRD, N₂ adsorption-desorption, TEM, EDS, XPS, and ICP-OES. Figure 1 displays the CO₂-TPD profiles of UiO-66 and UiO-66-NH₂. For UiO-66-NH₂, five peaks were observed when the desorption temperature was below 800 °C. The peaks located at 99 °C and 425 °C corresponded to weak basic sites and strong basic sites, respectively, while those peaks at 200 °C and 285 °C were ascribed to medium basic sites [53–56]. In addition, a strong peak at 547 °C is observed, originating from the decomposition of UiO-66-NH₂ [53–56]. However, only one CO₂ desorption peak (565 °C) appeared on the UiO-66 CO₂-TPD profile, which is attributed to the decomposition of UiO-66. This phenomenon was induced by

-NH_2 groups present on UiO-66-NH₂ [55]. CO₂-TPD characterization displayed a certain number of alkaline sites on UiO-66-NH₂, whereas no alkaline sites were found on UiO-66. The position and intense PXRD peaks of UiO-66 and UiO-66-NH₂ were in good agreement with those reported in literature, illustrating that the samples were synthesized successfully (Figure S1) [42,44,46]. Furthermore, the PXRD diffraction peaks of UiO-66 and UiO-66-NH₂ were the same because both have similar ligands (Figure S1) [44]. The peak position and intensity of PdNi/UiO-66-NH₂ (1:1), Pd/UiO-66-NH₂, PdNi/UiO-66 (1:1), and Pd/UiO-66 were similar to those of undeposited UiO-66 and UiO-66-NH₂, thus proving that the structures of UiO-66-NH₂ and UiO-66 were well maintained after the deposition of Pd-Ni NPs or Pd NPs (Figure S1). No characteristic peaks of Pd-Ni NPs, Pd NPs, and Ni NPs were observed in the PXRD patterns of PdNi/UiO-66-NH₂ (1:1) and PdNi/UiO-66 (1:1) due to the low Pd and Ni contents in the catalyst [57,58]. The adsorption/desorption isotherms of N₂ and textural properties on different samples are displayed in Figure S2 and Table 1. The sorption isotherms exhibited the type IV curves, suggesting that UiO-66, PdNi/UiO-66 (1:1), UiO-66-NH₂, and PdNi/UiO-66-NH₂ (1:1) possessed a mesoporous structure (Figure S2A). The BET surface areas of UiO-66, PdNi/UiO-66 (1:1), UiO-66-NH₂, and PdNi/UiO-66-NH₂ (1:1) were 1467, 1292, 1223, and 851 m²/g, respectively. The pore volume of UiO-66, PdNi/UiO-66 (1:1), UiO-66-NH₂, and PdNi/UiO-66-NH₂ (1:1) were 0.75 cm³/g, 0.70 cm³/g, 1.02 cm³/g, and 0.81 cm³/g, respectively. The BET surface area of UiO-66-NH₂ was smaller than UiO-66 because of the involvement of -NH_2 in the pores [40,42]. After the deposition of PdNi NPs on UiO-66 and UiO-66-NH₂, the pore volume and BET surface area decreased significantly, indicating that the addition of PdNi NPs resulted in a decrease in the pore volume and BET surface area of the UiO-66 and UiO-66-NH₂ [40]. The reduction in BET surface areas and pore volume is ascribed to the PdNi NPs occupying or blocking the pores of UiO-66 and UiO-66-NH₂ [59]. The UiO-66 and PdNi/UiO-66 (1:1) displayed a similar pore size distribution, and pore sizes are mainly distributed in 0.59, 0.82, 1.05, 1.25, and 3.21 nm. Moreover, UiO-66, after depositing PdNi NPs, presented a new pore size at 0.45 nm, which may be due to the involvement of PdNi NPs in the pores of UiO-66 (Figure S2B). The sample of UiO-66-NH₂ and PdNi/UiO-66-NH₂ (1:1) also presented similar pore size distributions, and a new pore size appeared at 0.35 nm (Figure S2C). However, the mean pore diameter increased after depositing PdNi NPs. The mean pore diameter of UiO-66, PdNi/UiO-66 (1:1), UiO-66-NH₂, and PdNi/UiO-66-NH₂ (1:1) was 2.1, 2.2, 3.3, and 3.8 nm, respectively. The increase of mean pore size of UiO-66 and UiO-66-NH₂ after depositing PdNi NPs was mainly because PdNi NPs could block the pores of UiO-66 and UiO-66-NH₂ [40]. TEM images of PdNi/UiO-66-NH₂ (1:1), Pd/UiO-66-NH₂, PdNi/UiO-66 (1:1), and Pd/UiO-66 revealed that the PdNi NPs or Pd NPs substantially dispersed on the surface of the UiO-66 and UiO-66-NH₂ support, with mean particle sizes of 4.6 nm, 7.7 nm, 7.1 nm, and 14.6 nm, respectively (Figures 2A,B, 3A,B and S3). The PdNi NPs or Pd NPs deposited on UiO-66-NH₂ are smaller than those deposited on UiO-66. Moreover, the particle size of PdNi NPs is smaller than that of Pd NPs when deposited on the same support. This may be because the amine group of UiO-66-NH₂ can act as an anchoring group to stabilize PdNi NPs or Pd NPs. In addition, the interaction between Pd and Ni could effectively prevent the aggregation of PdNi NPs. The EDS mapping analysis of PdNi/UiO-66-NH₂ (1:1) and PdNi/UiO-66 (1:1) displayed that Pd and Ni were evenly distributed in the catalysts (Figures 2C–F and 3C–F) [31,60]. As shown in Figures 2F and 3F, the overlap of Pd and Ni signal is not perfect, indicating that individual monometallic Pd and Ni NPs are formed on the surface of UiO-66 and UiO-66-NH₂ [39]. XPS measurement displayed that the Pd and Ni in the PdNi/UiO-66 (1:1) and PdNi/UiO-66-NH₂ (1:1) catalysts existed as metallic Pd (Pd⁰) and oxidation-state Ni (NiO) (Figure S4) [31,60,61]. The structure of the MOF support has no influence on the Pd and Ni valence state of PdNi/UiO-66-NH₂ (1:1) and PdNi/UiO-66 (1:1).

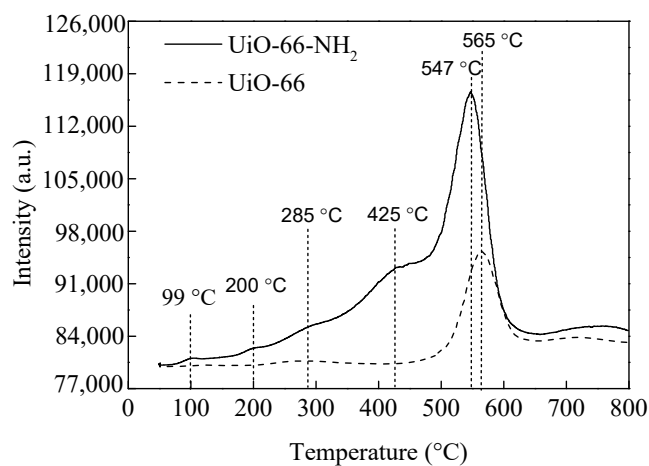


Figure 1. CO₂-TPD profiles for UiO-66-NH₂ and UiO-66.

Table 1. The textural properties of the samples.

Entry	Sample	BET (m ² /g)	Mean Pore Diameter (nm)	Volume (cm ³ /g)
1	UiO-66	1467	2.1	0.75
2	PdNi/UiO-66 (1:1)	1292	2.2	0.70
3	UiO-66-NH ₂	1223	3.3	1.02
4	PdNi/UiO-66-NH ₂ (1:1)	851	3.8	0.81

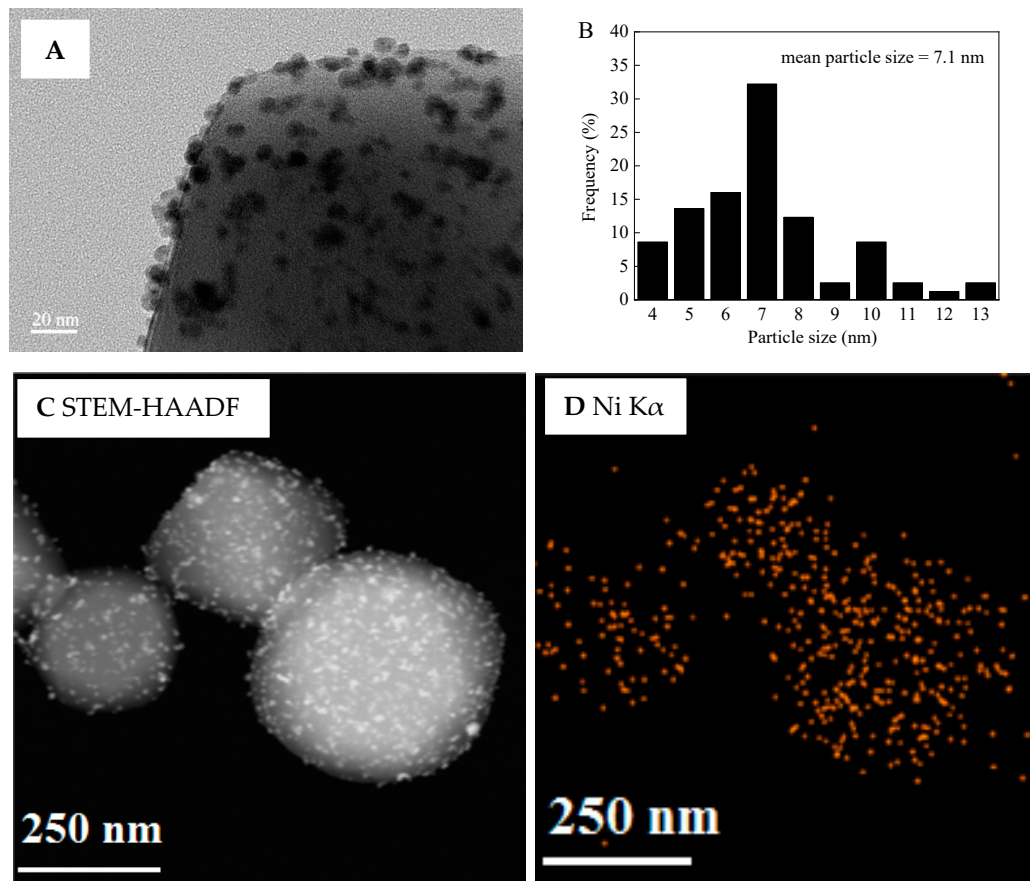


Figure 2. Cont.

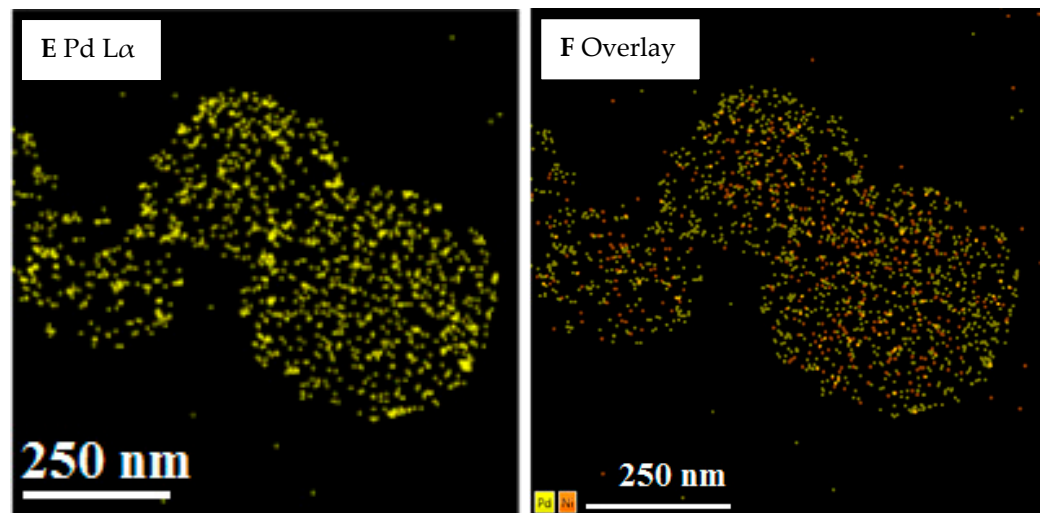


Figure 2. (A) TEM image, (B) PdNi size distribution, (C) STEM-HAADF image, and (D–F) EDS elemental mapping images of PdNi/UiO-66 (1:1).

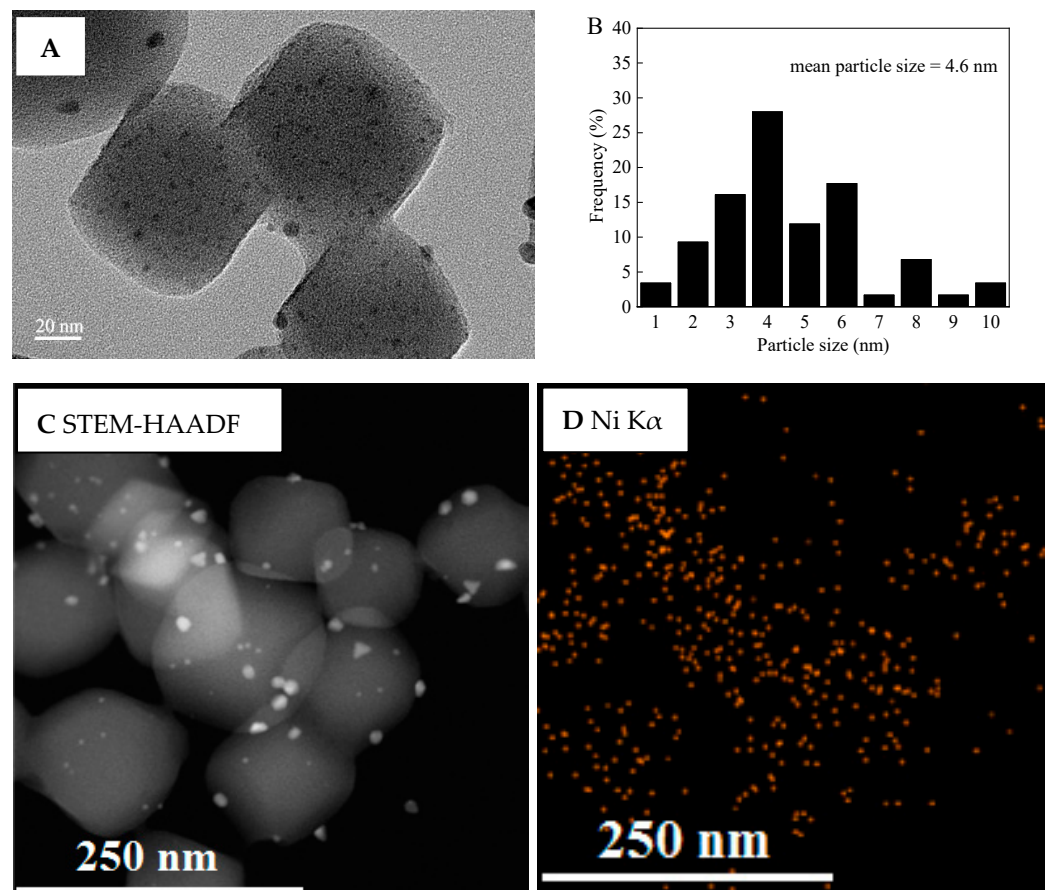


Figure 3. Cont.

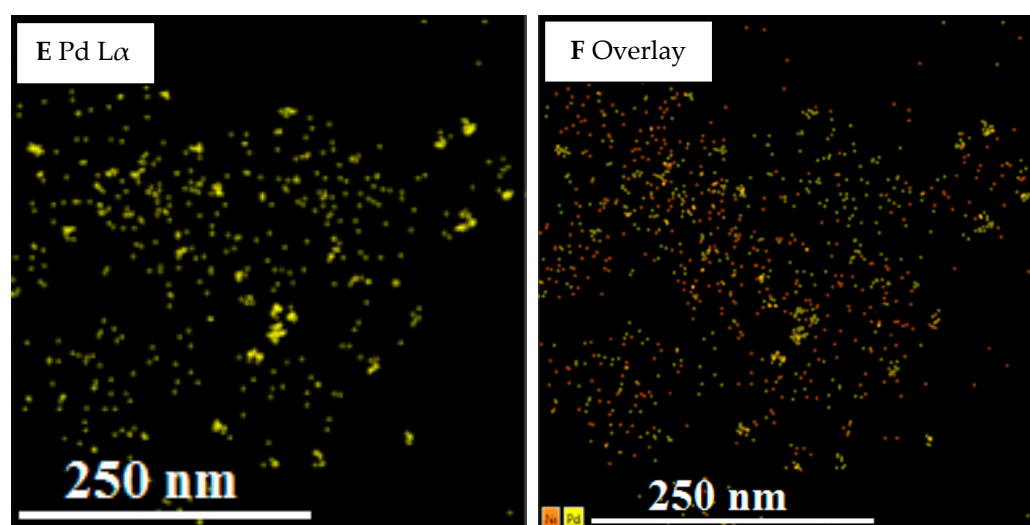


Figure 3. (A) TEM image, (B) PdNi size distribution, (C) STEM-HAADF image, and (D–F) EDS elemental mapping images of PdNi/UfO-66-NH₂ (1:1).

3.2. Catalytic Performance

UfO-66 and UfO-66-NH₂ MOFs were chosen to compare the influence of the support on the catalytic activity and selectivity for the selective hydrogenation of BD. The Pd–Ni bimetallic catalysts supported on UfO-66 and UfO-66-NH₂ were investigated in the BD hydrogenation reaction. The evolution of BD conversion and selectivity for PdNi/UfO-66 (1:1) and PdNi/UfO-66-NH₂ (1:1) in BD hydrogenation as a function of the reaction temperature (40–65 °C) are presented in Figure 4. The conversion of BD for UfO-66 and UfO-66-NH₂ supports are also illustrated in Figure 4. The supports of UfO-66 and UfO-66-NH₂ presented a low BD conversion of less than 1% at 40–65 °C (Figure 4A). The bimetallic PdNi/UfO-66 (1:1) catalysts exhibited higher catalytic activity than PdNi/UfO-66-NH₂ (1:1) (Figure 4A). A BD conversion of 99.8% was achieved on PdNi/UfO-66 (1:1) at 40 °C, and then it remained constant (Figure 4A). The BD conversion was only 15.6% for PdNi/UfO-66-NH₂ (1:1) at 40 °C. Then, it gradually increased with the increase in the reaction temperature, up to 100% at 60 °C (Figure 4A). The products of BD hydrogenation mainly include butane, 1-butene, *trans*-2-butene, and *cis*-2-butene, among which 1-butene, *trans*-2-butene, and *cis*-2-butene are the ideal products and butane is the by-product. For the PdNi/UfO-66 (1:1) catalyst, the selectivities to total butenes ranged between 61.5% and 84.5% and reduced when the temperature was increased to 60 °C from 40 °C (Figure 4B). A continuous reduction in the selectivity to 1-butene, *cis*-2-butene, and *trans*-2-butene was detected with the raise in temperature, whereas the selectivity to butane increased, suggesting that butenes were hydrogenated to produce butane on PdNi/UfO-66 (1:1) in the BD hydrogenation reaction (Figure 4B). Compared with PdNi/UfO-66 (1:1), PdNi/UfO-66-NH₂ (1:1) displayed different selectivities of butane and total butenes. For the PdNi/UfO-66-NH₂ (1:1) catalyst, the selectivity to butane and total butenes remained unchanged at low reaction temperatures (40 °C and 45 °C) (Figure 4C). However, the selectivity to total butenes was reduced slightly by raising temperature from 50 °C to 65 °C, whereas the selectivity to butane increased slightly (Figure 4C). The selectivities to butane and total butenes were 11.5% and 88.5%, 10.5% and 89.5%, 7.8% and 92.2%, 4.7% and 95.3%, 0.5% and 99.5%, and 0.7% and 99.3% at 65 °C, 60 °C, 55 °C, 50 °C, 45 °C, and 40 °C, respectively. The selectivity to total butenes (88.5–99.5%) on PdNi/UfO-66-NH₂ (1:1) was higher than that on PdNi/UfO-66 (1:1) (61.5–84.5%). The selectivity to 1-butene, *cis*-2-butene, and *trans*-2-butene were similar on PdNi/UfO-66-NH₂ (1:1) catalysts at low temperatures (40 °C and 45 °C), indicating that no isomerization was detected during BD hydrogenation at low temperature (Figure 4C) [21,31]. At high reaction temperatures (50–65 °C), the selectivity of 1-butene reduced with the raise of temperature, while that of *cis*-2-butene and *trans*-2-

butene improved with the raise of temperature (Figure 4C). This phenomenon indicated that 1-butene isomerized to *cis*-2-butene and *trans*-2-butene during BD hydrogenation at high reaction temperature [21,59]. The activity and selectivity of the Pd–Ni-supported catalysts were influenced critically by the structure of the MOF support. TEM characterization presented that the mean particle size of PdNi/UiO-66-NH₂ (1:1) (4.6 nm) is smaller than PdNi/UiO-66 (7.1 nm) due to the amine groups of UiO-66-NH₂. According to previously reported studies, the size of nanoparticles is the primary factor affecting the activity and selectivity for the BD hydrogenation reaction, and the catalyst with smallest NP size presented higher BD conversion [31]. However, the Pd-Ni NPs supported on UiO-66 was more active than that supported on UiO-66-NH₂. This could be due to the influence of MOF support structure. Compared with UiO-66, UiO-66-NH₂ with a certain number of alkaline sites could inhibit the catalytic activity for BD hydrogenation reaction. On the contrary, the alkaline environment of UiO-66-NH₂ is helpful to improve the butene selectivity. The selectivity of the PdNi/UiO-66 (1:1) to total produced butenes was approximately 84.5% at 99.8% BD conversion at 40 °C, while that of the PdNi/UiO-66-NH₂ (1:1) catalyst was 89.5% at 100% BD conversion at 60 °C (Figure 4B,C). These results are consistent with previous studies [40,62,63]. Zhang et al. [63] reported that Pd/Al₂O₃-TiO₂ catalyst modified with alkaline additive displayed better butene selectivity for the BD hydrogenation. Guan et al. [40] found that the structural differences between Pd-UiO-66-NH₂ and Pd-UiO-66 were the reasons for the different activities and the product selectivities of the two catalysts in the phenol hydrogenation. Liang et al. [62] reported that the photocatalytic activity of ZnTCPC/UIO-66(NH₂) with a stable covalent bond for methylene blue degradation was higher than that of ZnTCPC/UIO-66.

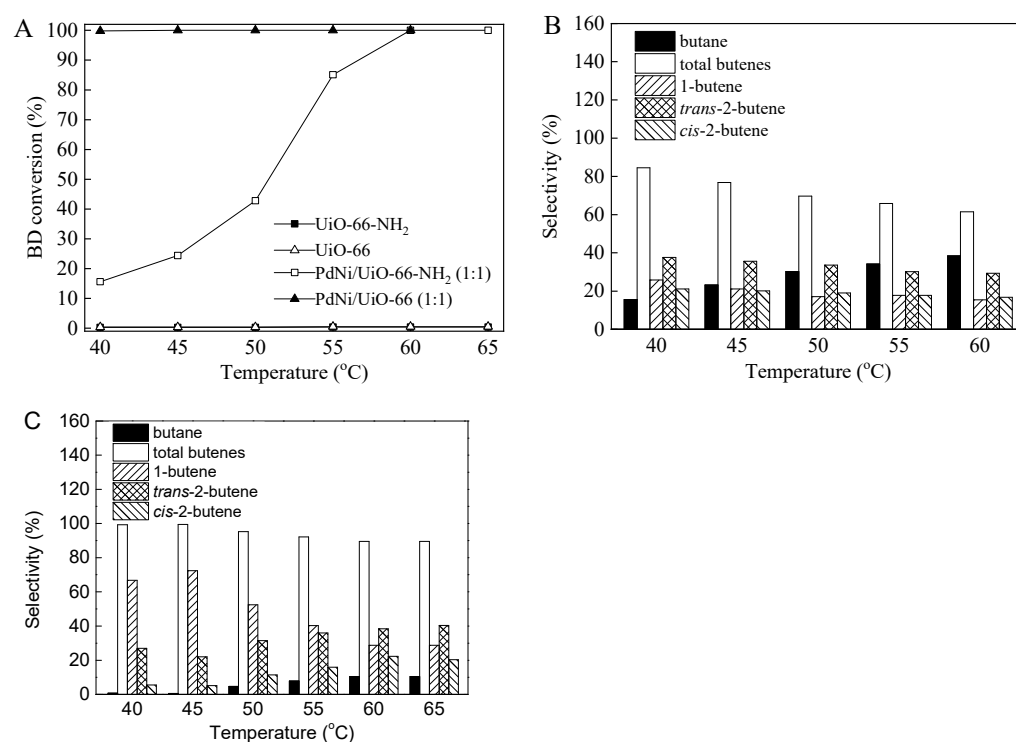


Figure 4. (A) BD conversions for UiO-66, UiO-66-NH₂, PdNi/UiO-66 (1:1) and PdNi/UiO-66-NH₂ (1:1); (B,C) Product selectivities for PdNi/UiO-66 (1:1) (B) and PdNi/UiO-66-NH₂ (1:1) (C) as a function of temperature (reaction conditions: 5 mg of catalyst, 6.5 mL/min of H₂ flow rate, 20 mL/min of 1.0 vol.%BD/N₂ flow rate. BD conversion and product selectivities given in (A–C) were stable data at reaction temperature).

In order to evaluate the catalytic performance of the synthesized catalyst in the BD hydrogenation, the BD conversion and selectivity to total butenes on different supported

Pd–Ni bimetallic catalysts were compared. The results are summarized in Table 2. PdNi/ γ -Al₂O₃ catalyst displayed good catalytic property, i.e., 90% conversion of BD and 80% selectivity of butenes at 70 °C [21]. The BD conversion and butene selectivity reached 85% and 100% at 70 °C on PdNi/SiO₂ catalyst [21]. Méndez et al. reported that 1NiPd/Al₂O₃ afforded excellent catalytic activity with a BD conversion and butene selectivity of 80% and 99.8% at 40 °C, respectively [29]. A complete BD conversion (100%) was achieved on 0.91%Pd1.51%Ni/ γ -Al₂O₃ catalyst at 87 °C [64]. Based on the above results, our PdNi/UiO-66 (1:1) and PdNi/UiO-66-NH₂ (1:1) catalysts display much higher catalyst activity and butene selectivity than PdNi/ γ -Al₂O₃ and 0.91%Pd1.51%Ni/ γ -Al₂O₃ for BD hydrogenation. Although the selectivity of PdNi/UiO-66 (1:1) and PdNi/UiO-66-NH₂ (1:1) is lower than that of PdNi/SiO₂, they display higher BD conversions at lower reaction temperatures. The PdNi/UiO-66 (1:1) catalyst shows higher BD conversions than 1NiPd/Al₂O₃ catalyst at 40 °C, but its selectivity of butene is smaller than 1NiPd/Al₂O₃. Although the BD conversion and butene selectivity of PdNi/UiO-66-NH₂ (1:1) are less than that of 1NiPd/Al₂O₃, the excellent stability (16 h) of the catalyst shows the advantage of using UiO-66-NH₂ as a support.

Table 2. The BD conversion and butene selectivity toward total butenes over supported Pd–Ni bimetallic catalysts for the BD hydrogenation reaction.

Entry	Catalyst	Mean Particle Size (nm)	T (°C)	Conv. (%)	Sel. (%)	Lifetime (h)	Ref.
1	PdNi/UiO-66 (1:1)	7.1	40	99.8	84.5	9	This work
2	PdNi/UiO-66-NH ₂ (1:1)	4.6	60	100	89.5	16	This work
3	PdNi/ γ -Al ₂ O ₃	5.9	70	90	80	-	21
4	PdNi/SiO ₂	6.3	70	85	100	-	21
5	1NiPd/Al ₂ O ₃	-	40	80	99.8	-	29
6	0.91%Pd1.51%Ni/ γ -Al ₂ O ₃	5.9	87	100	-	-	64

The molar ratio of the bimetallic metals presented a remarkable effect on the catalytic activity and selectivity in the hydrogenation of BD, because it affects the surface composition of bimetallic supported catalysts [1,15]. The effects of the Pd/Ni molar ratio of the PdNi/UiO-66 and PdNi/UiO-66-NH₂ catalysts on the BD conversions and product selectivities for the BD hydrogenation were investigated (Figures 5 and 6). For all the catalysts, the BD conversions and selectivities were found to be dependent on the molar ratio of Pd to Ni. The PdNi/UiO-66 catalyst with Pd/Ni ratios of 1:1, 2:1, and 3:1 displayed excellent BD conversions, reaching 99.8%, 100%, and 99.5% at 40 °C for the PdNi/UiO-66 (1:1), PdNi/UiO-66 (2:1), and PdNi/UiO-66 (3:1), respectively (Figure 5A). The BD conversions of PdNi/UiO-66 (1:3) and PdNi/UiO-66 (1:2) gradually increased with the increase in temperature; they were 99.6% and 99.8% at 70 °C and 55 °C for PdNi/UiO-66 (1:3) and PdNi/UiO-66 (1:2), respectively (Figure 5A). The selectivities of total produced butenes increased from 42.2% to 97.1% as the Pd/Ni molar ratio decreased from 3:1 to 1:3 at nearly 100% BD conversion (Figure 5B). Among all the tested PdNi/UiO-66 with different molar ratios, PdNi/UiO-66 (1:1) displays the highest catalytic activity and butene selectivity toward BD hydrogenation. For PdNi/UiO-66-NH₂, the catalytic activity (BD conversion) enhanced with the raise in the Pd/Ni molar ratio. PdNi/UiO-66-NH₂ (3:1) displayed the highest catalytic activity. A nearly complete BD conversion (99.7%) was achieved at 40 °C (Figure 6A). BD conversions of 98.4%, 95.1%, 100%, and 97.7% were achieved on PdNi/UiO-66-NH₂ (1:3), PdNi/UiO-66-NH₂ (1:2), PdNi/UiO-66-NH₂ (1:1), and PdNi/UiO-66-NH₂ (2:1) at 100 °C, 90 °C, 60 °C, and 55 °C, respectively (Figure 6A). The selectivities of total butenes were 87.7%, 80.8%, 89.5%, 72.8%, and 86.5% at nearly 100% BD conversion on PdNi/UiO-66-NH₂ (1:3), PdNi/UiO-66-NH₂ (1:2), PdNi/UiO-66-NH₂ (1:1), PdNi/UiO-66-NH₂ (2:1), and PdNi/UiO-66-NH₂ (3:1), respectively (Figure 6B). Although the PdNi/UiO-66-NH₂ (1:1) catalyst displayed moderate catalytic activity, the

excellent butene selectivity displayed that the PdNi/UiO-66-NH₂ catalyst with a Pd/Ni molar ratio of 1:1 rendered its optimal proportion.

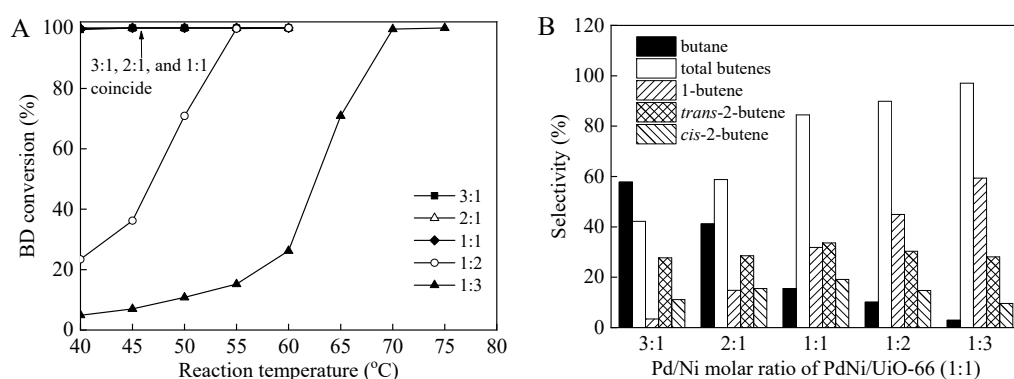


Figure 5. (A) BD conversions at different reaction temperature over PdNi/UiO-66 with diverse Pd/Ni molar ratios; (B) Product selectivities over PdNi/UiO-66 with diverse Pd/Ni molar ratios at nearly 100% BD conversion; (reaction conditions: 5 mg of catalyst, 6.5 mL/min of H₂ flow rate, 20 mL/min of 1.0 vol.%BD/N₂ flow rate. BD conversion and product selectivities given in (A,B) were stable data at reaction temperature).

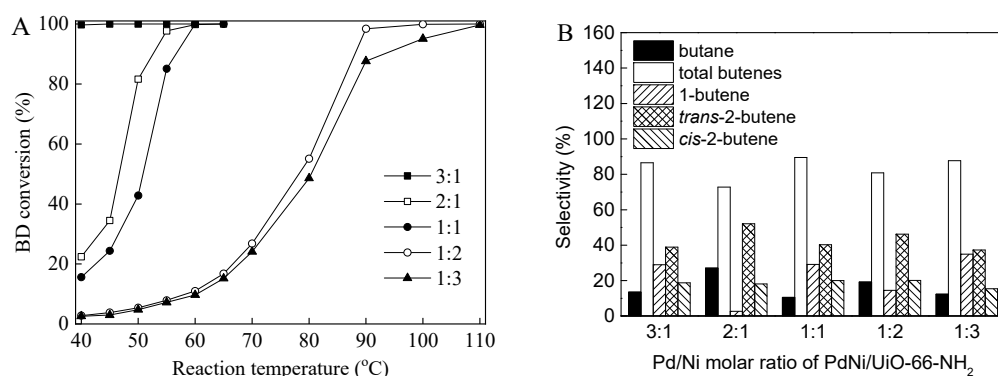


Figure 6. (A) BD conversions at different reaction temperature over PdNi/UiO-66-NH₂ with diverse Pd/Ni molar ratios; (B) Product selectivities over PdNi/UiO-66-NH₂ with diverse Pd/Ni molar ratios at nearly 100% BD conversion; (reaction conditions: 5 mg of catalyst, 6.5 mL/min of H₂ flow rate, 20 mL/min of 1.0 vol.%BD/N₂ flow rate. BD conversion and product selectivities given in (A,B) were stable data at reaction temperature).

The durability of PdNi/UiO-66 (1:1) and PdNi/UiO-66-NH₂ (1:1) was tested within a time on stream of 24 h at 40 °C and 55 °C, respectively. Figure 7 shows the time-on-stream effects on the BD conversion and product selectivity for PdNi/UiO-66 (1:1) and PdNi/UiO-66-NH₂ (1:1). The initial BD conversions of 99.8% and 85.3% were obtained for PdNi/UiO-66 (1:1) and PdNi/UiO-66-NH₂ (1:1), respectively (Figure 7A). For PdNi/UiO-66 (1:1), a steady BD conversion was obtained during the first 9 h time-on-stream. Then, the BD conversion decreases stepwise and the BD conversion was 54.2% after 24 h time-on-stream. The BD conversion remained constant for PdNi/UiO-66-NH₂ (1:1) during the first 16 h time-on-stream, and then the BD conversion gradually decreased from 85.3% to 58.8% with further extension of the time-on-stream from 16 h to 24 h. The PdNi/UiO-66-NH₂ (1:1) catalyst presented better stability than PdNi/UiO-66 (1:1) under the reaction conditions. This could be caused by the strong interaction between the -NH₂ groups of UiO-66-NH₂ and PdNi NPs. The selectivity to total butenes remained unchanged in the first 9 h and 16 h on PdNi/UiO-66 (1:1) and PdNi/UiO-66-NH₂ (1:1), respectively (Figure 7B,C). Moreover, the butene selectivity slightly increased with extension of the time-on-stream (Figure 7B,C).

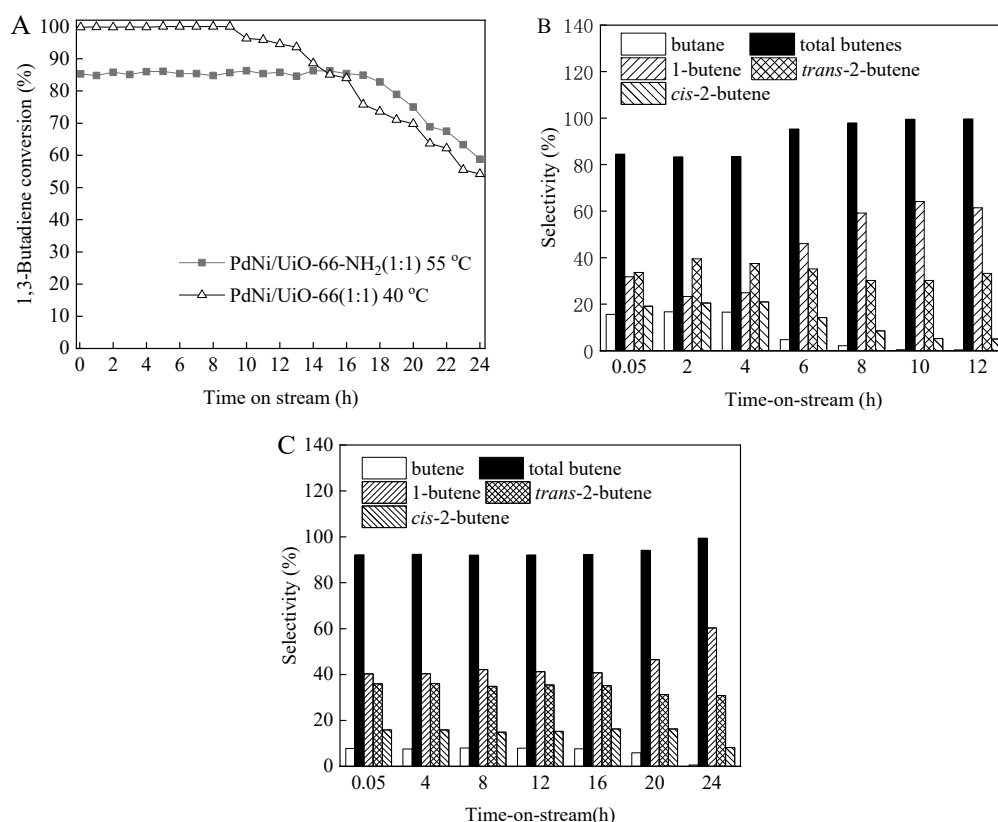


Figure 7. Evolution of the BD conversion and product selectivity with time-on-stream for PdNi/UiO-66 (1:1) and PdNi/UiO-66-NH₂ (1:1) at 40 °C and 55 °C, respectively: (A) BD conversion; (B) Product selectivity for PdNi/UiO-66 (1:1); (C) Product selectivity for PdNi/UiO-66-NH₂ (1:1) (reaction conditions: 5 mg of catalyst, 6.5 mL/min of H₂ flow rate, 20 mL/min of 1.0 vol.%BD/N₂ flow rate).

To evaluate the reproducibility of the catalyst, two batches of PdNi/UiO-66-NH₂ (1:1) catalysts were synthesized by the impregnation method. The catalytic activity and selectivity of the two batches of catalysts for the hydrogenation of BD were investigated under the same conditions (Figure S6). Two batches of PdNi/UiO-66-NH₂ (1:1) displayed similar BD conversions and product selectivities for the BD hydrogenation at 55 °C (Figure S6). PdNi/UiO-66-NH₂ (1:1) catalyst displayed good reproducibility.

Pd/UiO-66 and Pd/UiO-66-NH₂ presented a different catalytic property compared with Pd–Ni bimetallic catalysts (Figure S5). For Pd/UiO-66 catalyst, the conversion of BD was 90.2% at the initial stage of hydrogenation, and then quickly deactivated within 0.5 h. The BD conversion decreased to 13.9% at 50 °C for 12 h. However, there is a rise in selectivity to total butenes with increasing reaction time. The selectivity toward total butenes raised from 82.0% to 99.7% when the reaction time increased from 0.25 h to 8 h. Pd/UiO-66-NH₂ catalyst presented complete conversion at the initial stage of hydrogenation. The BD conversions slightly decreased in the next 4 h, and then rapidly decreased in the next 8 h, while the selectivity to total butenes steadily increased with the increase of the reaction time. The BD conversion and butene selectivity were 52.4% and 95% at 50 °C for 12 h, respectively. Obviously, the Pd NPs supported on UiO-66-NH₂ (100%) presented higher BD conversion than that supported on UiO-66 (90.2%). This result is contrary to those of Pd–Ni bimetallic catalysts. This may be explained by a previous study, which displayed that the catalysts with the smallest NP show higher BD conversion [31]. The TEM characterization shows that the Pd NP mean particle sizes were 14.6 nm and 7.7 nm for Pd/UiO-66 and Pd/UiO-66-NH₂, respectively. The catalytic activity for the hydrogenation of BD was dependent on both MOF support structure and particle size. Although the PdNi/UiO-66-NH₂ (1:1) bimetallic catalyst (42.8% BD conversion at 50 °C)

exhibited lower hydrogenation activity than Pd/UiO-66-NH₂ (100% BD conversions at 50 °C), it showed higher butene selectivity than monometallic Pd catalysts (95.3% and 51.8%). The PdNi/UiO-66 (1:1) (100%) displayed higher BD conversions than Pd/UiO-66 (90.2%), while the butene selectivity of the former (69.7%) was lower than the latter (82%). EDS characterization presented that Pd and Ni components existed as individual NPs in PdNi/UiO-66-NH₂ (1:1) and PdNi/UiO-66 (1:1) catalysts (Figures 2F and 3F). The improvement in the catalytic activity and selectivity of PdNi/UiO-66 (1:1) and PdNi/UiO-66-NH₂ (1:1) could be attributed to the synergistic effect between monometallic Pd NPs and Ni NPs. In addition, NH₂-doping enhances the catalyst stability, and the Pd/UiO-66-NH₂ (4 h) exhibits higher stability than Pd/UiO-66 (0.5 h). Compared with Pd/UiO-66-NH₂ and Pd/UiO-66 catalysts, Pd–Ni bimetallic catalysts PdNi/UiO-66 (1:1) and PdNi/UiO-66-NH₂ (1:1) displayed higher stability in the BD hydrogenation reaction, indicating that the interaction between Pd and Ni plays an important role in improving the stability of the catalyst.

4. Conclusions

A set of Pd–Ni or Pd catalysts supported on highly ordered MOFs of UiO-66 and UiO-66-NH₂ was successfully synthesized. TEM and EDS characterization displayed that PdNi NPs or Pd NPs were substantially dispersed on the surface of UiO-66-NH₂ and UiO-66. The interaction between –NH₂ groups of UiO-66-NH₂ and PdNi NPs or Pd NPs, as well as the interaction between Pd and Ni, can effectively prevent the aggregation of NPs. All catalysts were investigated in BD hydrogenation by using a fixed-bed, continuous-flow-type quartz reactor at 40–110 °C under ambient pressure. The results displayed that the structure of the MOF support, the molar ratio of Pd/Ni, and particle size have important effects on the catalytic activity and product selectivity. The UiO-66-NH₂ with a certain number of alkaline sites supporting Pd–Ni bimetallic NP catalysts displayed a lower catalytic activity than that of UiO-66 in the selective BD hydrogenation. However, they were more favorable to the formation of butenes. NH₂-doping and the synergistic interaction between Pd and Ni could enhance the catalyst stability. The bimetallic catalysts PdNi/UiO-66-NH₂ (1:1) (16 h) and PdNi/UiO-66 (1:1) (9 h) displayed higher stability than Pd/UiO-66-NH₂ (4 h) and Pd/UiO-66 (0.5 h). Moreover, the catalysts presented good reproducibility in the hydrogenation of BD. The bimetallic Pd–Ni catalysts with a Pd/Ni ratio of 1:1 demonstrated the best catalytic performance. These findings afford beneficial guidance for the design and preparation of high-efficiency catalysts for the selective hydrogenation of BD.

Supplementary Materials: The following supporting information can be downloaded at: <https://www.mdpi.com/article/10.3390/nano12091484/s1>, Figure S1: PXRD analysis of UiO-66, PdNi/UiO-66 (1:1), Pd/UiO-66, UiO-66-NH₂, PdNi/UiO-66-NH₂ (1:1), and Pd/UiO-66-NH₂; Figure S2: The N₂ adsorption-desorption isotherms (A) and pore size distribution (B,C) of UiO-66-NH₂, PdNi/UiO-66-NH₂(1:1), UiO-66, and PdNi/UiO-66(1:1); Figure S3: TEM images and Pd NP size distribution of Pd/UiO-66 (A,B) and PdNi/UiO-66-NH₂ (C,D); Figure S4: XPS spectra of PdNi/UiO-66-NH₂ (1:1) (A,B) and PdNi/UiO-66 (1:1) (C,D); Figure S5: Evolution of the BD conversion and product selectivity with time-on-stream for Pd/UiO-66 (A) and Pd/UiO-66-NH₂ (B) at 50 °C; Figure S6: Evolution of the BD conversion and product selectivity with time-on-stream for the first batch and second batch of PdNi/UiO-66-NH₂ (1:1) at 55 °C: (A) BD conversion; (B) Product selectivity for first batch; (C) Product selectivity for second batch; Table S1: The Pd and Ni weight content of Pd–Ni bimetallic catalysts.

Author Contributions: Conceptualization, L.L. and X.T.; methodology, L.L. and J.Z.; software, X.Z.; validation, L.Y., C.X. and Y.L.; formal analysis, L.L. and C.X.; investigation, S.S. and Z.L.; resources, L.L. and C.X.; data curation, X.Z.; writing—original draft preparation, L.L.; writing—review and editing, L.L., L.Y. and Y.L.; visualization, L.Y. and Y.L.; supervision, L.L. and X.T.; project administration, L.L.; funding acquisition, L.L., L.Y., X.Z., C.X. and Y.L. All authors have read and agreed to the published version of the manuscript.

Funding: This research was funded by the National Natural Science Foundation of China (grant number 21802104), the Natural Science Foundation of Shandong Province (grant number ZR2017MB056), High-tech Industrial Development Zone Science and Technology Huimin Plan of Weifang (grant number 2019KJHM18), and Technology Research and Development Program of Weifang (grant number 2021GX004 and 2021GX007).

Institutional Review Board Statement: Not applicable.

Informed Consent Statement: Not applicable.

Data Availability Statement: The data presented in this study are available on request from the corresponding author.

Conflicts of Interest: The authors declare no conflict of interest.

References

1. Yang, Q.; Hou, R.; Sun, K. Tuning butene selectivities by Cu modification on Pd-based catalyst for the selective hydrogenation of 1,3-butadiene. *J. Catal.* **2019**, *374*, 12–23. [[CrossRef](#)]
2. Yi, H.; Du, H.; Hu, Y.; Yan, H.; Jiang, H.L.; Lu, L. Precisely controlled porous alumina overcoating on Pd catalyst by atomic layer deposition: Enhanced selectivity and durability in hydrogenation of 1,3-butadiene. *ACS Catal.* **2015**, *5*, 2735–2739. [[CrossRef](#)]
3. Yang, Q.; Sun, K.; Xu, Y.; Ding, Z.; Hou, R. Tuning crystal phase of molybdenum carbide catalyst to induce the different selective hydrogenation performance. *Appl. Catal. A Gen.* **2022**, *630*, 118455–118465. [[CrossRef](#)]
4. Yardimci, D.; Serna, P.; Gates, B.C. A highly selective catalyst for partial hydrogenation of 1,3-butadiene: MgO-supported rhodium clusters selectively poisoned with CO. *ChemCatChem* **2012**, *4*, 1547–1550. [[CrossRef](#)]
5. Huang, Y.; Chen, Z.X. Alloying effect on the C–C coupling reactions in acetylene hydrogenation by palladium-coinage metal alloys, a DFT study and microkinetic modeling. *Appl. Surf. Sci.* **2022**, *575*, 151513–151521. [[CrossRef](#)]
6. Pattamakomsan, K.; Ehret, E.; Morfin, F.; Gélín, P.; Jugnet, Y.; Prakash, S.; Bertolini, J.C.; Panpranot, J.; Aires, F.J.C.S. Selective hydrogenation of 1,3-butadiene over Pd and Pd–Sn catalysts supported on different phases of alumina. *Catal. Today* **2011**, *164*, 28–33. [[CrossRef](#)]
7. Odoom-Wubah, T.; Li, Q.; Chen, M.; Fang, H.; Bediako, B.B.A.; Adilov, I.; Huang, J.; Li, Q. Influence of preparation methods on the catalytic activity of Pd–Cu/Mn₂O₃ catalyst in the hydrogenation of 1,3-butadiene. *ACS Omega* **2019**, *4*, 1300–1310. [[CrossRef](#)]
8. Chen, S.; Yang, B. Theoretical understandings on the unusual selectivity of 1,3-butadiene hydrogenation to butenes over gold catalysts. *Catal. Today* **2020**, *347*, 134–141. [[CrossRef](#)]
9. Hu, C.; Shao, M.; Xiang, M.; Li, S.; Xu, S. The role of hydrogen coverage and location in 1,3-butadiene hydrogenation over Pt/SiO₂. *React. Chem. Eng.* **2020**, *5*, 87–100. [[CrossRef](#)]
10. Hu, N.; Li, X.Y.; Liu, S.M.; Wang, Z.; He, X.K.; Hou, Y.X.; Wang, Y.X.; Deng, Z.; Chen, L.H.; Su, B.L. Enhanced stability of highly-dispersed copper catalyst supported by hierarchically porous carbon for long term selective hydrogenation. *Chin. J. Catal.* **2020**, *41*, 1081–1090. [[CrossRef](#)]
11. He, X.; Li, X.; Wang, Z.; Hu, N.; Deng, Z.; Chen, L.; Su, B. Self-reduction for the synthesis of Co supported on hierarchically porous carbon for selective hydrogenation reaction. *Chem. J. Chin. Univ. Chin.* **2020**, *41*, 639–645.
12. Feng, Y.; Zhou, L.; Wan, Q.; Lin, S.; Guo, H. Selective hydrogenation of 1,3-butadiene catalyzed by a single Pd atom anchored on graphene: The importance of dynamics. *Chem. Sci.* **2018**, *9*, 5890–5896. [[CrossRef](#)] [[PubMed](#)]
13. Bachiller-Baeza, B.; Iglesias-Juez, A.; Agostini, G.; Castillejos-López, E. Pd–Au bimetallic catalysts supported on ZnO for selective 1,3-butadiene hydrogenation. *Catal. Sci. Technol.* **2020**, *10*, 2503–2512. [[CrossRef](#)]
14. Hoeven, J.V.D.; Jelic, J.; Olthof, L.A.; Totarella, G.; Dijk-Moes, R.J.A.V.; Krafft, J.M.; Louis, C.; Studt, F.; Blaaderen, A.V.; Jongh, P.E.D. Unlocking synergy in bimetallic catalysts by core-shell design. *Nat. Mater.* **2021**, *20*, 1216–1220. [[CrossRef](#)] [[PubMed](#)]
15. Lu, F.; Sun, D.; Jiang, X. Plant-mediated synthesis of AgPd/γ-Al₂O₃ catalysts for selective hydrogenation of 1,3-butadiene at low temperature. *New J. Chem.* **2019**, *43*, 13891–13898. [[CrossRef](#)]
16. Ma, H.; Xu, X.; Xu, H.; Feng, H.; Yuan, X.; Cheng, D. Understanding composition-dependent catalytic performance of PdAg for the hydrogenation of 1,3-butadiene to 1-butene. *Catal. Commun.* **2021**, *149*, 106255–106260. [[CrossRef](#)]
17. Méndez, F.J.; Piccolo, L.; Solano, R.; Aouine, M.; Villasana, Y.; Guerra, J.; Curbelo, S.; Olivera-Fuentes, C.; Brito, J. Promoting effect of ceria on the performance of NiPd/CeO₂-Al₂O₃ catalysts for the selective hydrogenation of 1,3-butadiene in the presence of 1-butene. *New J. Chem.* **2018**, *42*, 11165–11173. [[CrossRef](#)]
18. Aguilar-Tapia, A.; Delannoy, L.; Louis, C.; Han, C.W.; Ortalan, V.; Zanella, R. Selective hydrogenation of 1,3-butadiene over bimetallic Au-Ni/TiO₂ catalysts prepared by deposition-precipitation with urea. *J. Catal.* **2016**, *344*, 515–523. [[CrossRef](#)]
19. Lucci, F.R.; Liu, J.; Marcinkowski, M.D.; Yang, M.; Allard, L.F.; Flytzani-Stephanopoulos, M.; Sykes, E.C.H. Selective hydrogenation of 1,3-butadiene on platinum-copper alloys at the single-atom limit. *Nat. Commun.* **2015**, *6*, 8550–8557. [[CrossRef](#)]
20. Huang, X.; Yan, H.; Huang, L.; Zhang, X.; Lin, Y.; Li, J.; Xia, Y.; Ma, Y.; Sun, Z.; Wei, S.; et al. Toward understanding of the support effect on Pd1 single-atom-catalyzed hydrogenation reactions. *J. Phys. Chem. C* **2019**, *123*, 7922–7930. [[CrossRef](#)]
21. Hou, R.; Porosoff, M.D.; Chen, J.G.; Wang, T. Effect of oxide supports on Pd–Ni bimetallic catalysts for 1,3-butadiene hydrogenation. *Appl. Catal. A Gen.* **2015**, *490*, 17–23. [[CrossRef](#)]

22. Decarolis, D.; Lezcano-Gonzalez, I.; Gianolio, D.; Beale, A.M. Effect of particle size and support type on Pd catalysts for 1,3-butadiene hydrogenation. *Top. Catal.* **2018**, *61*, 162–174. [[CrossRef](#)] [[PubMed](#)]
23. Lonergan, W.W.; Wang, T.; Vlachos, D.G.; Chen, J.G. Effect of oxide support surface area on hydrogenation activity: Pt/Ni bimetallic catalysts supported on low and high surface area Al₂O₃ and ZrO₂. *Appl. Catal. A Gen.* **2011**, *408*, 87–95. [[CrossRef](#)]
24. Wang, T.; Mpourmpakis, G.; Lonergan, W.W.; Vlachos, D.G.; Chen, J.G. Effect of oxide supports in stabilizing desirable Pt–Ni bimetallic structures for hydrogenation and reforming reactions. *Phys. Chem. Chem. Phys.* **2013**, *15*, 12156–12164. [[CrossRef](#)]
25. Selvakannan, P.R.; Hoang, L.; Kumar, V.V.; Dumbre, D.; Jampaiah, D.; Das, J.; Bhargava, S.K. Selective hydrogenation of 1,3-butadiene to 1-butene: Review on catalysts, selectivity, kinetics and reaction mechanism. *Catal. Clean Energy Environ. Sustain.* **2021**, *495*, 205–228.
26. Lonergan, W.W.; Vlachos, D.G.; Chen, J.G. Correlating extent of Pt–Ni bond formation with low-temperature hydrogenation of benzene and 1,3-butadiene over supported Pt/Ni bimetallic catalysts. *J. Catal.* **2010**, *271*, 239–250. [[CrossRef](#)]
27. Cai, F.; Yang, L.; Shan, S.; Mott, D.; Chen, B.; Luo, J.; Zhong, C.J. Preparation of PdCu alloy nanocatalysts for nitrate hydrogenation and carbon monoxide oxidation. *Catalysts* **2016**, *6*, 96. [[CrossRef](#)]
28. Insorn, P.; Kitiyanan, B. Selective hydrogenation of concentrated vinyl acetylene mixed C₄ by modified Pd catalysts: Effect of Cu. *Catalysts* **2016**, *6*, 199. [[CrossRef](#)]
29. Méndez, F.J.; Solano, R.; Villasana, Y.; Guerra, J.; Curbelo, S.; Inojosa, M.; Olivera-Fuentes, C. Selective hydrogenation of 1,3-butadiene in presence of 1-butene under liquid phase conditions with NiPd/Al₂O₃ catalysts. *Appl. Petrochem. Res.* **2016**, *6*, 379–387. [[CrossRef](#)]
30. Wang, Z.; Wang, G.; Louis, C.; Delannoy, L. Novel non-noble bimetallic Cu–Zn/TiO₂ catalysts for selective hydrogenation of butadiene. *J. Catal.* **2017**, *347*, 185–196. [[CrossRef](#)]
31. Liu, L.; Zhou, X.; Guo, L.; Yan, S.; Li, Y.; Jiang, S.; Tai, X. Bimetallic Au–Pd alloy nanoparticles supported on MIL-101(Cr) as highly efficient catalysts for selective hydrogenation of 1,3-butadiene. *RSC Adv.* **2020**, *10*, 33417–33427. [[CrossRef](#)]
32. Singh, B.K.; Lee, S.; Na, K. An overview on metal-related catalysts: Metal oxides, nanoporous metals and supported metal nanoparticles on metal organic frameworks and zeolites. *Rare Met.* **2020**, *39*, 751–766. [[CrossRef](#)]
33. Wei, Z.H.; Zhang, R.R.; Mu, L.N.; Huang, Y.P.; Liu, Z.S. Fabrication of core-shell sol-gel hybrid molecularly imprinted polymer based on metal–organic framework. *Eur. Polym. J.* **2019**, *121*, 109301–109308. [[CrossRef](#)]
34. Zhang, Y.; Yu, W.D.; Zhao, C.F.; Yan, J. Dimensional reduction of Eu-based metal-organic framework as catalysts for oxidation catalysis of C(sp³)–H bond. *Chin. J. Chem.* **2022**, *40*, 480–486. [[CrossRef](#)]
35. Vakili, R.; Slater, T.J.A.; Hardacre, C.; Walton, A.S.; Fan, X. PtNi bimetallic structure supported on UiO-67 metal-organic framework (MOF) during CO oxidation. *J. Catal.* **2020**, *391*, 522–529. [[CrossRef](#)]
36. Liu, P.; Gu, X.; Wu, Y.; Cheng, J.; Su, H. Construction of bimetallic nanoparticles immobilized by porous functionalized metal-organic frameworks toward remarkably enhanced catalytic activity for the room-temperature complete conversion of hydrous hydrazine into hydrogen. *Int. J. Hydrogen Energy* **2017**, *42*, 19096–19105. [[CrossRef](#)]
37. Liu, L.; Zhou, X.; Yan, Y.; Zhou, J.; Zhang, W.; Tai, X. Bimetallic gold-silver nanoparticles supported on zeolitic imidazolate framework-8 as highly active heterogeneous catalysts for selective oxidation of benzyl alcohol into benzaldehyde. *Polymers* **2018**, *10*, 1089. [[CrossRef](#)]
38. Yu, J.H.; Yu, J.; Wei, Z.C.; Guo, X.M.; Mao, H.F.; Mao, D.S. Preparation and characterization of UiO-66-supported Cu–Ce bimetal catalysts for low-temperature CO oxidation. *Catal. Lett.* **2019**, *149*, 496–506. [[CrossRef](#)]
39. Ten, S.; Torbina, V.V.; Zaikovskii, V.I.; Kulinich, S.A.; Vodyankina, O.V. Bimetallic AgPd/UiO-66 hybrid catalysts for propylene glycol oxidation into lactic acid. *Materials* **2020**, *13*, 5471. [[CrossRef](#)]
40. Guan, Q.; Wang, B.; Chai, X.; Liu, J.; Gu, J.; Ning, P. Comparison of Pd–UiO-66 and Pd–UiO-66–NH₂ catalysts performance for phenol hydrogenation in aqueous medium. *Fuel* **2017**, *205*, 130–141. [[CrossRef](#)]
41. Jiang, Y.; Liu, C.; Caro, J.; Huang, A. A new UiO-66–NH₂ based mixed-matrix membranes with high CO₂/CH₄ separation performance. *Microporous Mesoporous Mater.* **2019**, *274*, 203–211. [[CrossRef](#)]
42. Liu, R.; Meng, S.; Ma, Y.; Niu, L.; He, S.; Xu, X.; Su, B.; Lu, D.; Yang, Z.; Lei, Z. Atmospheric oxidative coupling of amines by UiO-66–NH₂ photocatalysis under milder reaction conditions. *Catal. Commun.* **2019**, *124*, 108–112. [[CrossRef](#)]
43. Bai, Y.; Dou, Y.; Xie, L.H.; Rutledge, W.; Li, J.R.; Zhou, H.C. Zr-based metal-organic frameworks: Design, synthesis, structure, and applications. *Chem. Soc. Rev.* **2016**, *45*, 2327–2367. [[CrossRef](#)] [[PubMed](#)]
44. Lv, G.; Liu, J.; Xiong, Z.; Zhang, Z.; Guan, Z. Selectivity adsorptive mechanism of different nitrophenols on UiO-66 and UiO-66–NH₂ in aqueous solution. *J. Chem. Eng. Data* **2016**, *61*, 3868–3876. [[CrossRef](#)]
45. Cseri, L.; Hardian, R.; Anan, S.; Vovusha, H.; Schwingenschlögl, U.; Budd, P.M.; Sada, K.; Kokado, K.; Szekeley, G. Bridging the interfacial gap in mixed-matrix membranes by nature-inspired design: Precise molecular sieving with polymer-grafted metal–organic frameworks. *J. Mater. Chem. A* **2021**, *9*, 23793–23802. [[CrossRef](#)]
46. Zhu, H.; Huang, J.; Zhou, Q.; Lv, Z.; Li, C.; Hu, G. Enhanced luminescence of NH₂-UiO-66 for selectively sensing fluoride anion in water medium. *J. Lumin.* **2019**, *208*, 67–74. [[CrossRef](#)]
47. Kiracki, K.; Bůžek, D.; Peer, P.; Liška, V.; Mosinger, J.; Křížová, I.; Kloda, M.; Ondrušová, S.; Lang, K.; Demel, J. Polymeric membranes containing iodine-loaded UiO-66 nanoparticles as water-responsive antibacterial and antiviral surfaces. *ACS Appl. Nano Mater.* **2022**, *5*, 1244–1251. [[CrossRef](#)]

48. Guo, Z.; Xiao, C.; Maligal-Ganesh, R.V.; Zhou, L.; Goh, T.W.; Li, X.; Tesfagaber, D.; Thiel, A.; Huang, W. Pt nanoclusters confined within metal-organic framework cavities for chemoselective cinnamaldehyde hydrogenation. *ACS Catal.* **2014**, *4*, 1340–1348. [[CrossRef](#)]
49. Yoshimaru, S.; Sadakiyo, M.; Maeda, N.; Yamauchi, M.; Kato, K.; Pirillo, J.; Hijikata, Y. Support effect of metal-organic frameworks on ethanol production through acetic acid hydrogenation. *ACS Appl. Mater. Interfaces* **2021**, *13*, 19992–20001. [[CrossRef](#)]
50. Stawowowy, M.; Ciesielski, R.; Maniecki, T.; Matus, K.; Łużny, R.; Trawczynski, J.; Silvestre-Albero, J.; Łamacz, A. CO₂ hydrogenation to methanol over Ce and Zr containing UiO-66 and Cu/UiO-66. *Catalysts* **2020**, *10*, 39. [[CrossRef](#)]
51. Primet, M.; El Azhar, M.; Guenin, M. Influence of the support towards platinum catalysed 1,3-butadiene hydrogenation. *Appl. Catal.* **1990**, *58*, 241–253. [[CrossRef](#)]
52. Chakarova, K.; Strauss, I.; Mihaylov, M.; Drenchev, N.; Hadjiivanov, K. Evolution of acid and basic sites in UiO-66 and UiO-66-NH₂ metal-organic frameworks: FTIR study by probe molecules. *Microporous Mesoporous Mater.* **2019**, *281*, 110–122. [[CrossRef](#)]
53. Wang, G.N.; Chen, L.M.; Guo, Y.Y.; Fu, M.L.; Wu, J.L.; Huang, B.C.; Ye, D.Q. Effect of chromium doping on the catalytic behavior of Cu/ZrO₂/CNTs-NH₂ for the synthesis of methanol from carbon dioxide hydrogenation. *Acta Phys. Chim. Sin.* **2014**, *30*, 923–931.
54. Xu, L.; Wang, Q.; Liang, D.; Wang, X.; Lin, L.; Cui, W.; Xu, Y. The promotions of MnO and K₂O to Fe/silicalite-2 catalyst for the production of light alkenes from CO₂ hydrogenation. *Appl. Catal. A Gen.* **1998**, *173*, 19–25. [[CrossRef](#)]
55. Zheng, X.X.; Shen, L.J.; Chen, X.P.; Zheng, X.H.; Au, C.T.; Jiang, L.L. Amino-modified Fe-terephthalate metal-organic framework as an efficient catalyst for the selective oxidation of H₂S. *Inorg. Chem.* **2018**, *57*, 10081–10089. [[CrossRef](#)]
56. Ewald, S.; Hinrichsen, O. On the interaction of CO₂ with Ni-Al catalysts. *Appl. Catal. A Gen.* **2019**, *580*, 71–80. [[CrossRef](#)]
57. Liu, L.L.; Zhou, X.J.; Liu, L.; Jiang, S.; Li, Y.J.; Guo, L.X.; Yan, S.J.; Tai, X.S. Heterogeneous bimetallic Cu–Ni nanoparticle-supported catalysts in the selective oxidation of benzyl alcohol to benzaldehyde. *Catalysts* **2019**, *9*, 538. [[CrossRef](#)]
58. Liu, L.; Zhang, X.; Rang, S.; Yang, Y.; Dai, X.; Gao, J.; Xu, C.; He, J. Catalysis by metal-organic frameworks: Proline and gold functionalized MOFs for the aldol and three-component coupling reactions. *RSC Adv.* **2014**, *4*, 13093–13107.
59. Liu, L.; Tai, X.; Zhou, X.; Liu, L.; Zhang, X.; Ding, L.; Zhang, Y. Au-Pt bimetallic nanoparticle catalysts supported on UiO-67 for selective 1,3-butadiene hydrogenation. *J. Taiwan Inst. Chem. Eng.* **2020**, *114*, 220–227. [[CrossRef](#)]
60. Liu, L.L.; Tai, X.S.; Zhou, X.J.; Hou, J.X.; Zhang, Z.H. Bimetallic Au-Ni alloy nanoparticles in a metal-organic framework (MIL-101) as efficient heterogeneous catalysts for selective oxidation of benzyl alcohol into benzaldehyde. *J. Alloys Compd.* **2019**, *790*, 326–336. [[CrossRef](#)]
61. Shi, Y.; Yang, H.; Zhao, X.; Cao, T.; Chen, J.; Zhu, W.; Yu, Y.; Hou, Z. Au–Pd nanoparticles on layered double hydroxide: Highly active catalyst for aerobic oxidation of alcohols in aqueous phase. *Catal. Commun.* **2012**, *18*, 142–146. [[CrossRef](#)]
62. Liang, Q.; Zhang, M.; Zhang, Z.; Liu, C.; Xu, S.; Li, Z. Zinc phthalocyanine coupled with UIO-66 (NH₂) via a facile condensation process for enhanced visible-light-driven photocatalysis. *J. Alloys Compd.* **2017**, *690*, 123–130. [[CrossRef](#)]
63. Zhang, K.; Kong, T.; Zeng, Y.; Tan, Z. Effect of support modified by a alkaline additive on the properties of Pd/Al₂O₃-TiO₂ catalysts. *Pet. Process. Petrochem.* **2011**, *42*, 38–42.
64. Hou, R.; Yu, W.; Porosoff, M.D.; Chen, J.G.; Wang, T. Selective hydrogenation of 1,3-butadiene on PdNi bimetallic catalyst: From model surfaces to supported catalysts. *J. Catal.* **2014**, *316*, 1–10. [[CrossRef](#)]